

FLIGHT PERFORMANCE ANALYSIS OF ELECTRIC AIRCRAFT UNDER MOTOR FAILURE CONDITIONS USING REDUCED-ORDER MODELING

Luca Hein[1] & Stephan Myschik[1]

[1]University of the Bundeswehr Munich, Institute for Aeronautical Engineering, Werner-Heisenberg-Weg 39, Neubiberg, 85577, Bavaria, Germany

Abstract

This paper presents a reduced-order modeling approach for electric motor components to be used in flight performance analysis of electric aircraft under failure conditions. The derivation of certification-relevant flight and mission performance data is a key challenge in the development of electrically powered aircraft, while high-fidelity electric motor models are computationally unsuitable for mission-level simulations. To overcome this limitation, a data-driven reduced-order motor model is developed and integrated into a closed-loop, 6-degrees-of-freedom aircraft dynamics simulation. The reduced-order model captures the essential behavior of the electric propulsion system in both nominal and fault operation while significantly reducing computational effort. The simulation framework is coupled with an automated, certification-oriented flight performance and requirements validation toolchain. The approach is demonstrated using a fault-tolerant electric propulsion system developed within the ELAPSED project. Results for take-off performance under failure scenarios are evaluated against EASA Certification Specification CS-22 requirements.

Keywords: flight performance, reduced-order modeling, electric aircraft, motor failure operation

1. Motivation and State of the Art

The development of new aircraft, and in particular, electrically powered propulsion systems, requires a comprehensive flight performance analysis of novel products. For certification purposes, this analysis must cover not only nominal operating conditions but also relevant failure scenarios. Such investigations are typically conducted using simulations of varying fidelity, depending on the development stage and the specific analysis objectives.

For flight performance analysis covering missions, including multiple flight phases and abnormal operating conditions, the direct use of high-fidelity electric motor models is often impractical. In the present case, the available electric motor model operates at a sampling rate of $100\,\mathrm{kHz}$, which leads to excessive computational effort when coupled with aircraft-level simulations over long time horizons. Consequently, this level of detail is not suitable for system-level flight performance studies. A reduced-order model that captures the relevant dynamic behavior of the electric motor in both normal and fault operation represents a more appropriate solution, with a clear focus on computational efficiency while retaining sufficient accuracy.

The research project ELAPSED [1] addresses the development of a novel propulsion system for an electrically powered motor glider. The propulsion system comprises a 5-phase permanent-magnet synchronous machine (PMSM) combined with a fault-tolerant motor control architecture [2] and [3]. An open-loop high-fidelity simulation model of the electric motor is already available and is thoroughly discussed in [4]. Within the scope of this work, the primary interest lies in the resulting aircraft flight performance under both nominal and fault-induced motor operating conditions.

The state of the art regarding electric machines and fault-tolerant control strategies for PMSMs is comprehensively discussed in [2], [3], and [4]. Furthermore, the increasing relevance of reduced-order modeling approaches and machine learning techniques for the modeling of PMSMs is outlined in [5]. The theoretical foundations of reduced-order modeling can be found in [6] and [7]. There are various techniques and approaches for building reduced-order models (ROMs), depending on the intended application and the inherent trade-off between computational effort and model accuracy, as described in [8] and [9]. For the present use case, the emphasis is explicitly placed on computational efficiency rather than maximum model fidelity.
In [10], an approach for a flux-linkage-based PMSM-ROM using artificial neural networks and machine learning techniques is presented, which is comparable to the method employed in this paper. Kiss [11] focuses on selecting the most suitable method depending on the desired implementation.
Based on this background, the contributions of this paper are threefold: first, a detailed 6-degrees-of-freedom flight performance analysis of an electric aircraft under motor fault conditions is conducted; second, a closed-loop aircraft dynamics simulation is established that integrates a reduced-order electric motor model; and third, a systematic reduced-order modeling process is presented for generating neural state-space models derived from a high-fidelity electric motor model.

2. Methodology

The methodology applied in this work follows a structured, model-based approach that systematically bridges the gap between component-level high-fidelity simulations and aircraft-level flight performance analysis. The overall objective is to enable efficient and robust mission-level simulations while preserving the essential dynamic characteristics of the electric propulsion system, including fault behavior. The general workflow adopted in this study can be summarized as follows:

1. A high-fidelity reference model of the electric propulsion system is employed, exemplified by an electric motor model operating at a sampling rate of $100\,\mathrm{kHz}$. This model serves as the ground truth and is capable of accurately representing both nominal and fault conditions of the motor.

2. Based on simulation data generated by the high-fidelity model, a reduced-order model (ROM) is derived. The training data cover the relevant operating envelope, including different operating points and fault scenarios. The ROM generation process comprises the selection of suitable model structures, learning algorithms, and hyperparameters tailored to the intended application.

3. After successful validation (see Figure 2 and Subsection 4.2), the resulting ROM is integrated into the aircraft flight performance simulation environment. In this setup, the ROM is executed at the same sampling rate as the flight dynamics model ($200\,\mathrm{Hz}$), ensuring numerical consistency and efficient coupling within the closed-loop aircraft simulation.

4. Finally, the integrated simulation framework is used to perform automated flight performance analysis and requirements validation. This includes the systematic evaluation of mission performance and compliance with relevant performance requirements under both nominal and motor failure conditions.

This methodology enables a scalable and computationally efficient assessment of electric aircraft flight performance while maintaining clear traceability to the underlying high-fidelity propulsion system model.

3. Reduced-Order Modeling

"Reduced-order modeling is a technique for simplifying full order high-fidelity models by reducing their computational complexity, while preserving their dominant behavior." [12]
In this paper, a reduced-order model (ROM) is used as an implementation method for the electric machine – a permanent magnet synchronous motor (PMSM). Reduced-order models enable a significant improvement in computational efficiency while preserving the dominant system dynamics. Fundamentals regarding ROMs can be found in [6] and [7]. Since a high-fidelity electric motor model is available, a data-driven ROM approach is adopted in this work. The high-fidelity motor model investigated in [4] operates at a maximum rotational speed of $2500\ \mathrm{rpm}$ and a maximum load torque

of $250\ \mathrm{Nm}$ under normal conditions. In the event of an open-phase fault, these values decrease to approximately $2300\ \mathrm{rpm}$ and $140\ \mathrm{Nm}$, as 1 phase is no longer operational. The fault-tolerant control strategy presented in [2], [3], and [4] maintains motor operability under this fault condition, but only within these reduced limits. The model is controlled by the user through the commanded rotational speed, load torque, and fault parameters. When combined with a propeller, the load torque is provided by the propeller itself since the propeller rotational speed and the torque required to sustain that speed are directly correlated. To ensure broad applicability of the ROM, the motor is trained in isolation, i.e., without a propeller. This enables flexible coupling with different propeller models, independent of the specific application or aircraft configuration.
For the intended flight performance analysis, only a limited set of motor inputs and outputs is required. Relevant inputs are the commanded rotational speed, the propeller-induced torque load, and the operational mode (normal or fault operation). The outputs of interest comprise the actual rotational speed, the generated torque, and the electrical power demand. Detailed internal quantities such as phase currents, field weakening states, or rotational acceleration are neglected in the ROM, as they are not required at the aircraft performance level. All other relevant data, such as mechanical power, efficiency, or overall current, can be calculated based on the ROM outputs.
The ROM is formulated as a nonlinear state-space model according to [7]:

$$\begin{cases} \dot{\mathbf{x}} = \mathbf{f}(\mathbf{x}(t), \mathbf{u}(t), t, \theta_1) \\ \mathbf{y} = \mathbf{g}(\mathbf{x}(t), \mathbf{u}(t), t, \theta_2) \end{cases}, \tag{1}$$

where $\mathbf{x}$ denotes the state vector, $\mathbf{u}$ the input vector, t the time, $\mathbf{y}$ the output vector, and $\theta_{1/2}$ the parameter vectors.
The ROM generation process consists of the following steps:

1. *Data generation*: The high-fidelity motor model is simulated over an extended time horizon (e.g., $800\,\mathrm{s}$) using randomly varying inputs within the motor's operating range (0–$2500\,\mathrm{rpm}$ and 0–$250\,\mathrm{Nm}$) and under both normal and fault conditions to generate representative training and validation datasets.

2. *Data preparation*: The simulation data is postprocessed by sorting and normalizing (e.g., using the z-score method according to [13]) to achieve faster convergence, and is optionally downsampled.

3. *Data splitting*: The dataset is divided into separate training and validation subsets. This step is essential, as the ROM must be validated using data that was not employed during training. Otherwise, the model may merely reproduce the training data accurately without demonstrating the ability to generalize to previously unseen operating conditions and input trajectories. In this work, the overall data of $800\,\mathrm{s}$ simulation time are split in half, resulting in $400\,\mathrm{s}$ training data and $400\,\mathrm{s}$ validation data.

4. *Neural state-space identification*:

   (a) Definition of ROM inputs, outputs, and the neural state-space model structure.

   (b) Segmentation of the training data into fixed-length sequences to improve training robustness. For the intended application, a sequence size of 20 samples is chosen since larger segments rapidly increase the training effort, while smaller sequence sizes fail to capture the motor dynamics effectively.

   (c) Selection of algorithm settings, including solver, maximum number of epochs, and input interpolation method.

   (d) Training of the neural state-space model, yielding the final ROM. The evolution of the training loss is shown in Figure 1. The loss evolution indicates numerically stable training without signs of divergence or instability. A final loss function value of 0.015 indicates that the ROM has learned the motor behavior properly.

5. *Model validation*: The ROM is validated against independent high-fidelity motor simulation data to assess accuracy. Therefore, the validation data specified in *data splitting* is used. Figure 2 illustrates the validation results against original validation data, which was not used to train the model. The ROM achieves accuracies ranging from above 97% to nearly 99%, depending on the state. This shows the high accuracy of the ROM in comparison to the original high-fidelity model. As the data are normalized as 'z-scores' with a mean value of 0, there are also negative values for rotational speed, torque, and electric power.

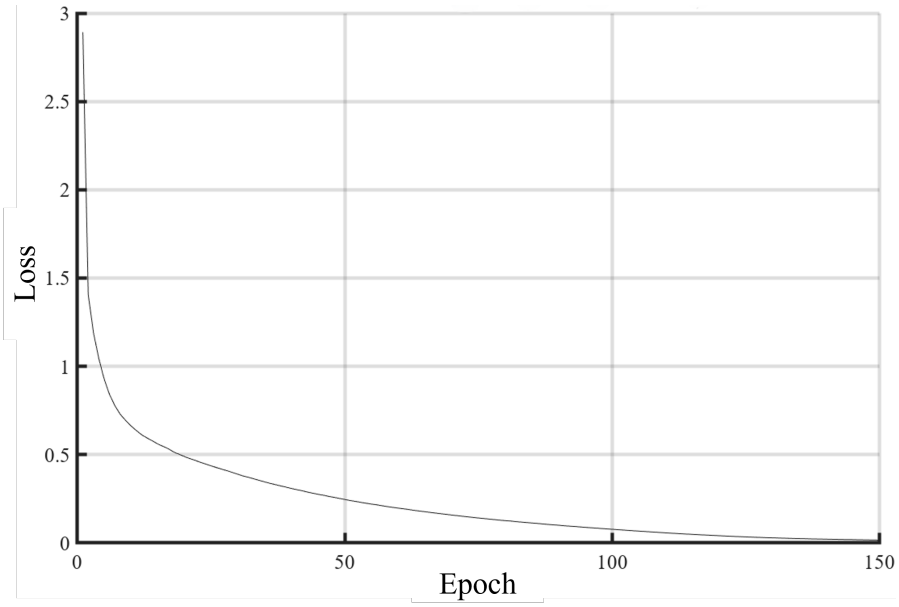


Figure 1 – Training loss (mean-squared error) of the neural state network.

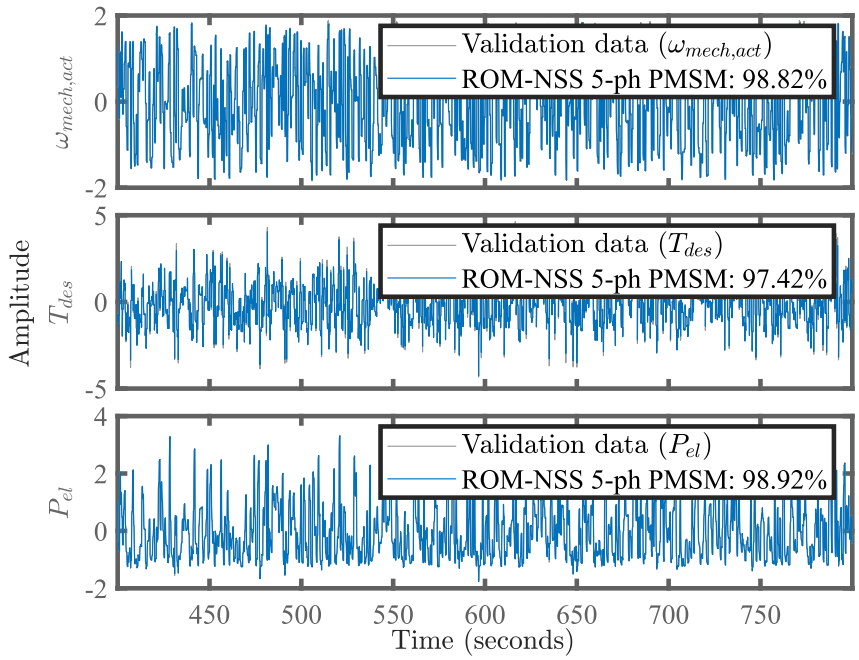


Figure 2 – Validation results of the reduced-order motor model against original normalized validation data.

Overall, the reduced-order model increases simulation performance by a factor of approximately 300 (500 simulation seconds require $3.3\,\mathrm{s}$ using the ROM compared to $1000\,\mathrm{s}$ with the high-fidelity model).

4. Flight Performance Analysis

4.1 General Setup and Vehicle

The flight performance analysis is conducted within an automated requirements validation toolchain, as described in [14]. This framework enables a certification-compliant and automated assessment of aircraft performance by validating simulation results against predefined performance requirements, such as take-off distance. The flight dynamics model, shown in Figure 3, is a six-degree-of-freedom aircraft simulation that includes models of the environment, aerodynamics, landing gear, weight and balance, battery system, engine, and propulsion system. For the present analysis, the previous engine model (highlighted by the red rectangle), which is limited to normal operation, is replaced by the ROM to enable simulation of motor operation under open-phase fault conditions.

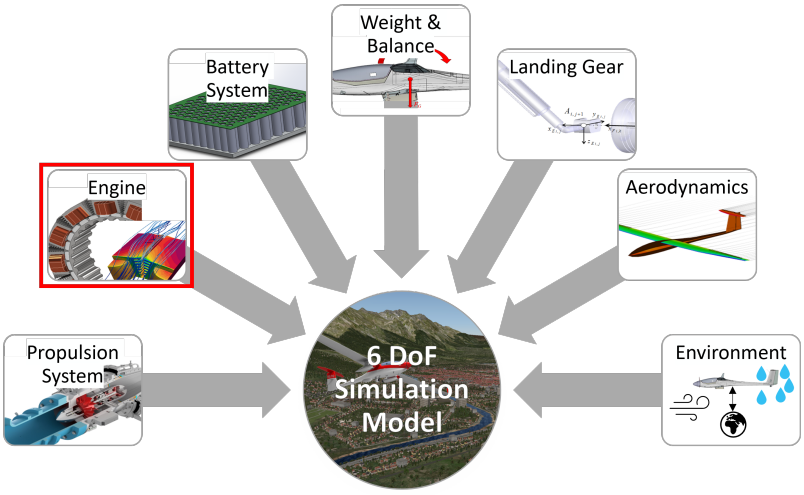


Figure 3 – flight dynamics model including components

The aircraft under consideration for the following flight performance analysis is an electrically powered motor glider with a wingspan of $20\ \mathrm{m}$ and a total aircraft weight of $820\ \mathrm{kg}$, which includes a battery system weighing $120\ \mathrm{kg}$. The battery is made of MOLICEL INR-21700-P42A cells [15] and utilizes multilevel technology, which promises several advantages in terms of performance and safety, as found in [16] and [17]. The novel propulsion system is based on a project-internally developed motor and a clipped Helix H50F 1.45 m R-SI-14 [18] propeller, generating a maximum shaft power of $65\ \mathrm{kW}$ at a rotational speed of $2500\ \mathrm{rpm}$ and $250\ \mathrm{Nm}$ torque.

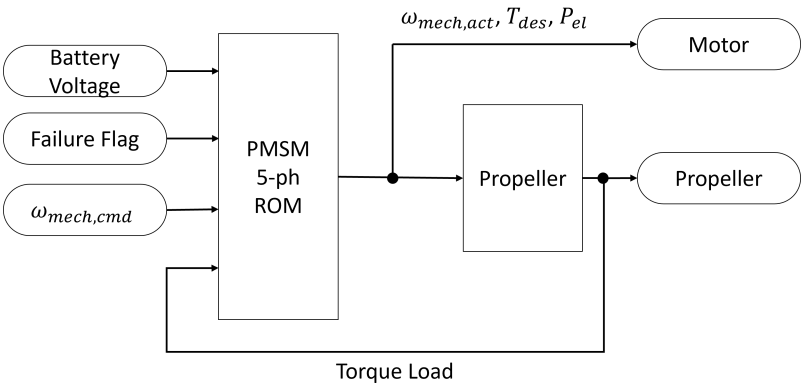


Figure 4 – Simulink model structure of PMSM 5-phase ROM and propeller.

Figure 4 shows the Simulink model structure of the motor ROM and the propeller, which are integrated into the overall aircraft simulation (see Figure 3). Inputs to this propulsion system are the provided battery voltage, the failure flag, and the commanded rotational speed of the motor-propeller combination. For both the motor and the propeller, torque and speed must be in equilibrium, which is why the propeller torque is fed back into the motor as a torque load. The maximum torque and speed

that the motor can provide both limit the power output of the motor-propeller combination, analogous to a real physical connection via the motor shaft. Further relevant data, such as the current drawn from the battery system, are also calculated within this model and provided to other aircraft systems via the system outputs.

4.2 Validation of Reduced-order Model against Aircraft Simulation

In Section 3., the motor ROM was already validated against high-fidelity motor simulation data based on the model of Ackermann [4]. In this section, the new ROM-based motor model and the baseline engine model are integrated into the aircraft simulation to validate the ROM by comparing their takeoff performance. However, this is only possible for nominal, failure-free operation, as the baseline motor model is limited to representing only normal operation.

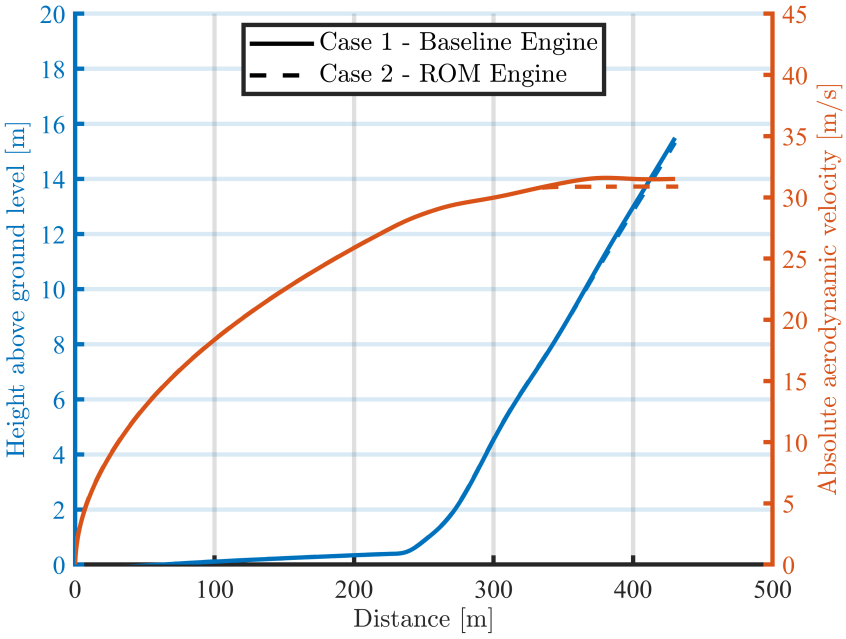


Figure 5 – Validation of ROM against baseline engine.

Motor Model	Take-off Distance	Execution Time
Baseline Engine	424 m (100%)	2.7 s (100%)
ROM Engine	426 m (100.5%)	3.2 s (119%)

Table 1 – Results of validation: ROM against baseline engine

Figure 5 shows a representative take-off procedure for both the baseline engine model and the ROM-based motor. The blue lines represent the height above ground level, and the orange lines represent the absolute aerodynamic velocity. Both configurations yield the same acceleration and, therefore, the same take-off distance, with a discrepancy of less than $2\,\mathrm{m}$. The small change in airspeed (less than $0.5\,\mathrm{m/s}$) that starts at a distance of $340\,\mathrm{m}$ – when the aircraft has already taken off and is climbing – is caused by the interaction and responsiveness of the simulation models, the reactive pilot model, and the control algorithms, and can be neglected in this case. Regarding simulation performance, both models achieve comparable results. The baseline engine model completes the automated take-off approximately $0.4\,\mathrm{s}$ faster, requiring $2.7\,\mathrm{s}$, whereas the ROM requires $3.2\,\mathrm{s}$. Although this corresponds to a nearly 20% increase in execution time, both models are still at least an order of magnitude faster than real time, given that the actual take-off duration was approximately $35\,\mathrm{s}$. This demonstrates that the ROM provides an excellent match to the baseline engine model under nominal operating conditions. The advantage of the ROM is that it supports motor failure operation, which justifies the slightly higher computational effort compared with the baseline engine.

4.3 Operation Cases and Results

Table 2 summarizes the motor operating conditions. Case 1 corresponds to nominal motor operation. Cases 2 to 4 represent an open-phase failure of the 5-phase electric machine occurring at aircraft velocities of $27\,\mathrm{m/s}$, $28.9\,\mathrm{m/s}$, and $0\,\mathrm{m/s}$, respectively. The failure onset speeds in cases 2 and 3 are chosen to coincide with the aircraft lift-off velocity. For motor failures induced at lower aircraft velocities, i.e., speeds below the decision speed, the pilot would abort the take-off. In case 4, it is assumed that the pilot is unaware of the motor failure, for example, because the failure indication is malfunctioning, and the motor already has an open-phase failure at the beginning of the acceleration phase.

Case Number	Failure Description	Failure Occurrence (Aircraft Velocity)
Case 1	No failure	–
Case 2	Open-phase failure	27 m/s
Case 3	Open-phase failure	28.9 m/s
Case 4	Open-phase failure	0 m/s

Table 2 – Simulated motor operation cases

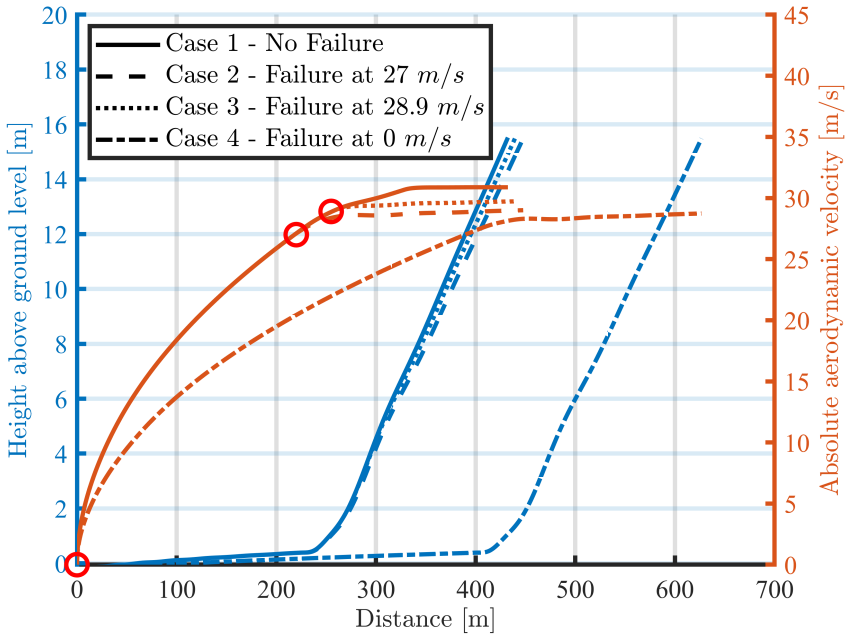


Figure 6 – Take-off distance for normal and failure cases of motor operation (acc. to Table 2).

Figure 6 shows the take-off performance for nominal motor operation and for the 3 motor-failure scenarios described in Table 2. The orange curves denote the aircraft's true airspeed, while the blue curves indicate the height above ground. When the lift-off speed of approximately $29\,\mathrm{m/s}$ is reached, the reactive pilot, as described in [19] and [20], commands an elevator deflection to initiate lift-off and subsequently controls the climb angle. The red circles mark the onset of motor failures for cases 2 to 4. Relative to nominal operation, all failure scenarios exhibit an increased take-off distance, particularly for failures occurring early on, because the maximum available thrust (see Figure 7) is reduced due to decreased maximum rotational speed and torque, resulting in lower aircraft acceleration.
Figure 7 shows the time history of the propeller thrust generated by the propulsion system for all cases. After an initialization period of $10\,\mathrm{s}$, the acceleration phase begins with a full-throttle command. The maximum thrust depends on the instantaneous aerodynamic speed of the aircraft, which causes the thrust to vary during the acceleration phase. The red circles again mark the occurrence of motor failure. In case 4, the failure occurs immediately at the start of take-off, leading to a reduced thrust level. In cases 2 and 3, the failure is triggered at higher speeds, occurring later in time but resulting

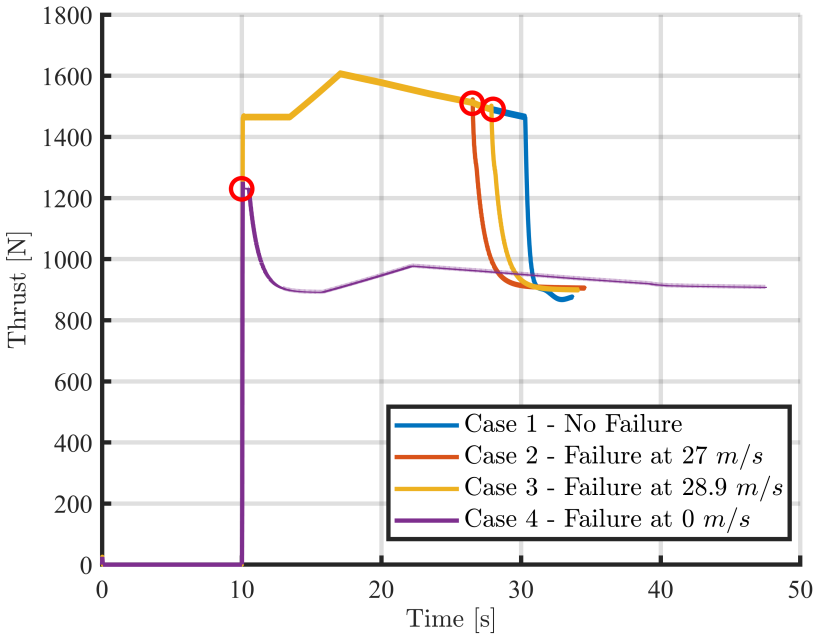


Figure 7 – Propeller thrust for normal and failure cases of motor operation (acc. to Table 2).

in the same thrust level after failure. In the nominal case, the maximum thrust also decreases at approximately 30 s into the simulation. This reduction is not caused by a failure but by a lower throttle setting, since the aircraft has already reached climb speed and the commanded climb angle. To maintain this speed, a thrust of about 900 N is required, which is approximately equal to the maximum thrust available in the failure cases. The take-off in case 4 takes roughly 10 s longer than in cases 1 to 3 due to slower aircraft acceleration from reduced maximum thrust.

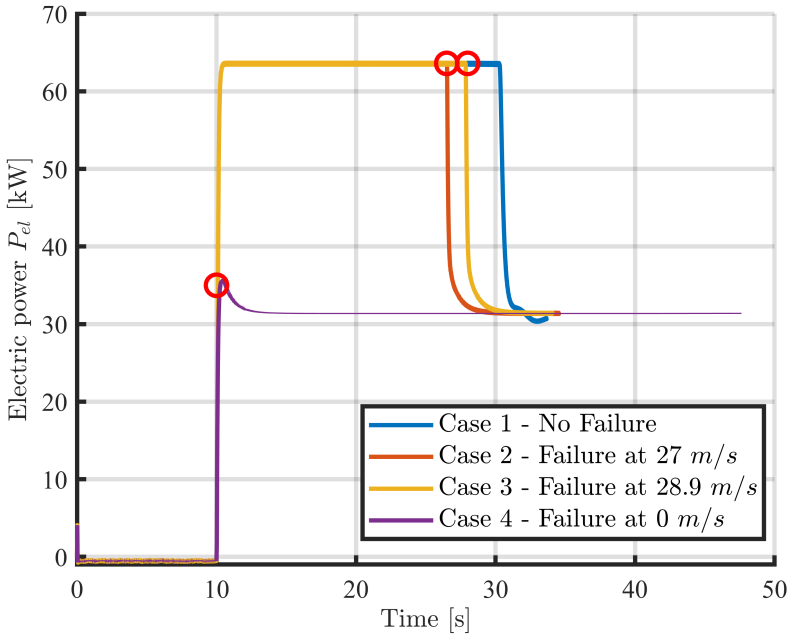


Figure 8 – Electric power for normal and failure cases of motor operation (acc. to Table 2).

Comparable to the thrust, the electric power behaves accordingly, as shown in Figure 8. After initialization, the electric power increases to a maximum value of around 65 kW. Upon the occurrence of an open-phase failure, the maximum electric power drops to nearly 32 kW.
According to the EASA certification specification CS-22 [21], the take-off distance is defined as the

ground distance from standstill to a height of $15\,\mathrm{m}$ above ground level and must not exceed $500\,\mathrm{m}$ for aircraft in this category. The take-off speed must also be maintained in the event of engine failure but may be lower, with a minimum value of 115% of the stall speed, whereas the nominal take-off speed must be 130% of the stall speed. As shown in Figure 6, the aircraft satisfies the take-off distance requirement in cases 1 to 3. In case 4, where the open-phase failure occurs at the beginning of the take-off run, the limit is exceeded, with a take-off distance of $620\,\mathrm{m}$. In all cases, however, the aircraft is able to maintain the required airspeed, even in failure scenarios. The results of the requirements validation are summarized in Table 3, including the achieved take-off distances.

Case Number	Failure Description	Failure Occurrence	Take-off Distance	Test Passed
Case 1	No failure	–	426 m	✓
Case 2	Open-phase failure	27 m/s	441 m	✓
Case 3	Open-phase failure	28.9 m/s	433 m	✓
Case 4	Open-phase failure	0 m/s	620 m	×

Table 3 – Results for take-off distance of simulated motor operation cases (acc. to Table 2)

5. Conclusion and Outlook

In this work, a data-driven reduced-order model for an electric motor is developed and integrated into a closed-loop, 6-degrees-of-freedom aircraft dynamics simulation. This framework enables flight and mission performance analysis of electric aircraft under nominal and motor failure conditions, allowing engineers to systematically study a wide range of realistic operational scenarios. It captures the essential behavior of the electric propulsion system in both nominal and faulted operation while greatly reducing computational effort, making certification-relevant mission-level simulations feasible and scalable to large scenario sets. The results show a validation rate above 97% for the reduced-order model relative to the high-fidelity motor model. The approach has been demonstrated on a fault-tolerant electric propulsion system from the ELAPSED project, and take-off performance results under failure scenarios have been evaluated with respect to EASA CS-22 requirements, showing the suitability of the method for supporting regulatory compliance assessments and early-stage design decisions.

Future work will focus on extending the reduced-order modeling framework to a broader range of propulsion architectures and fault types. Further refinement of the data-driven modeling strategies and validation against higher-fidelity models and experimental data will enhance prediction accuracy, robustness, and training performance. In addition, integrating more comprehensive certification criteria and operational scenarios into the automated validation toolchain will strengthen its applicability to the design and certification of next-generation electric aircraft. Finally, deploying the reduced-order model on a hardware-in-the-loop platform will be investigated to enable real-time assessment and control of propulsion system performance under realistic operating conditions.

6. Contact Author Email Address

The corresponding author can be reached at: luca.hein@unibw.de

7. Copyright Statement

The authors confirm that they, and/or their company or organization, hold copyright on all of the original material included in this paper. The authors also confirm that they have obtained permission, from the copyright holder of any third party material included in this paper, to publish it as part of their paper. The authors confirm that they give permission, or have obtained permission from the copyright holder of this paper, for the publication and distribution of this paper as part of the ICAS proceedings or as individual off-prints from the proceedings.

Acknowledgments

This research and project ELAPSED are funded by dtec.bw – Digitalization and Technology Research Center of the Bundeswehr. dtec.bw is funded by the European Union – NextGenerationEU. [1]

References

[1] dtec.bw. Electric Aircraft Propulsion – die Zukunft der Flugzeugantriebe, 08.11.2022.

[2] Martin Ackermann, José-Luis Marqués, and Claus Hillermeier. Optimal multi-fault tolerant control for PMSMs – Part I: Feedforward control. In *2024 IEEE 21st International Power Electronics and Motion Control Conference (PEMC)*, pages 1–9. IEEE, 2024.

[3] Martin Ackermann, José-Luis Marqués, and Claus Hillermeier. Optimal multi-fault tolerant control for PMSMs – Part II: Feedback control. In *2024 IEEE 21st International Power Electronics and Motion Control Conference (PEMC)*, pages 1–7. IEEE, 2024.

[4] Martin Ackermann. *Optimal multi-fault tolerant control for PMSMs*. Dissertation, Universität der Bundeswehr München, December 2025.

[5] Md. Ali Azom, Md. Shahen Hossain, and Md. Yakub Ali Khan. Review of Electrical and Thermal Modeling Techniques for Three-Phase PMSM Drives. *Control Systems and Optimization Letters*, 3:75–83, 2025.

[6] John Eason, Lorenz Biegler, B. Lohmann, Tamara Bechtold, P. Eberhard, Jörg Fehr, D. Rixen, Maria Cruz Varona, Christopher Lerch, Chengdong Yuan, E. Rudnyi, B. Fröhlich, P. Holzwarth, D. Grunert, Christian Meyer, Johannes Rutzmoser, Elke Deckers, Wim Desmet, and Bernard Haasdonk. *Model Order Reduction: Volume 3 Applications*. 2020.

[7] Maria Cruz Varona. *Model Reduction of Nonlinear Dynamical Systems by System-Theoretic Methods*. Dissertation, Technische Universität München, November 2020.

[8] Ram Kumar and D. Ezhilarasi. A state-of-the-art survey of model order reduction techniques for large-scale coupled dynamical systems. *International Journal of Dynamics and Control*, 11(2):900–916, 2023.

[9] Weihua Huang, Jin Wang, Junchen Zhao, Libing Zhou, and Zhiwei Zhang. Demagnetization Analysis and Magnet Design of Permanent Magnet Synchronous Motor for Electric Power Steering Applications. In *2020 IEEE 1st China International Youth Conference on Electrical Engineering (CIYCEE)*, pages 1–6, 2020.

[10] Maria Raluca Raia, Mircea Ruba, Raul Octavian Nemes, and Claudia Martis. Artificial Neural Network and Data Dimensionality Reduction Based on Machine Learning Methods for PMSM Model Order Reduction. *IEEE Access*, 9:102345–102354, 2021.

[11] Kristóf Levente Kiss and Tamás Orosz. Model Order Reduction Methods for Rotating Electrical Machines: A Review. *Energies*, 17(20):5145, 2024.

[12] MathWorks – Maker of MATLAB and Simulink, 10.04.2024.

[13] Sinan Ozdemir and Divya Susarla. *Feature engineering made easy: Identify unique features from your dataset in order to build powerful machine learning systems*. PACKT Publishing, Erscheinungsort nicht ermittelbar, 1st ed. edition, 2018.

[14] Luca Hein, Purav Panchal, and Stephan Myschik. Certification compliant performance analysis and requirements management of an electrically powered general aviation aircraft. *Journal of Aeronautics and Space Technologies*, 17(Special Issue):208–218, 2024.

[15] MOLICEL. Data sheet MOLICEL INR-21700-P42A, 08.08.2023.

[16] Johannes Buberger, Anton Kersten, Manuel Kuder, Arthur Singer, Ali Mashayekh, Julian Estaller, Torbjorn Thiringer, Richard Eckerle, and Thomas Weyh. Charging strategy for battery electric vehicles with a battery modular multilevel management (bm3) converter system using a pr controller. In *2021 23rd European Conference on Power Electronics and Applications (EPEECCE Europe)*. IEEE, 2021.

[17] Nina Sorokina, Tobias Högerl, Bliemetsrieder Wolfgang, Luca Hein, Thomas Weyh, and Manuel Kuder. Investigation of reconfigurable battery efficiency for an application in an electrical sailplane. In *2023 25th European Conference on Power Electronics and Applications (EPE'23 ECCE Europe)*, pages 1–8. IEEE, 2023.

[18] Helix-Carbon GmbH. Helix propeller, 2023.

[19] Nico Sauert. *Entwicklung eines Missionsautopiloten zur automatisierten Untersuchung von Flugleistungen*. Bachelorarbeit, Universität der Bundeswehr, München, 2022.

[20] Luca Hein, Purav Panchal, Denis Surmann, and Stephan Myschik. Requirements Validation for Electric Aircraft Under Adverse Flying Conditions. In *AIAA AVIATION FORUM AND ASCEND 2024*, Reston, Virginia, 2024. American Institute of Aeronautics and Astronautics.

[21] European Aviation Safety Agency. CS-22 Amendment 3: Certification Specifications, Acceptable Means of Compliance and Guidance Material for Sailplanes and Powered Sailplanes, 15.09.2021.